7. Electron stimulated desorption (ESD)

7.1 Introduction

When CaF_2 crystals are irradiated with electrons of sufficient energy, a strong emission of energetic F^+ ions is observed. The question whether this emission is due to the Knotek-Feibelman process or not has been discussed controversially in literature. The desorption threshold predicted by the Knotek-Feibelman process (28 eV for CaF_2) was established experimentally by three groups [MSS91], [ZGT94], [CDV94]. However, the important question of desorbing ion kinetic energies is still open, which is crucial for a detailed understanding of the desorption process. In earlier investigations performed on bulk crystals, ion kinetic energies were obscured by positive sample charging, while measurements on thin films gave contradicting results.

In the first part of this chapter, a new method is developed that allows the determination of a positive surface potential of ionic crystals under electron irradiation. For crystals cleaved in UHV, a new transient behavior of the surface potential during the first 30 min of irradiation was found that was not observed for crystals cleaved in air. The surface potential is closely connected to the surface stoichiometry of the crystal under irradiation and to charge transport in the crystal.

The method for surface charge determination is used to obtain for the first time the F^+ kinetic energy distribution for bulk CaF_2 crystals corrected for surface charge. An influence of changes in surface stoichiometry induced by dosage of O_2 and CO_2 on the charge corrected ion kinetic energy is demonstrated.

It is demonstrated that the electric field inside the charged crystal is important for the transport of fluorine to the surface, and hence for the temporal evolution of the F^+ ion yield under irradiation. For comparison, desorption from thin CaF_2 films evaporated on Si (111) was investigated. The main difference between crystals and films in the context of this investigation is the lack of surface charging for the latter. Field driven diffusion does not contribute to the desorption yield, and indeed a different temporal evolution of the desorption yield is observed.

7.2. Surface potential determination

7.2.1 Introduction

In electron irradiation of insulating samples, surface charging is observed. From an experimentalist point of view, charging is a nuisance in many standard surface science techniques involving the detection of charged particles like electrons or ions. A correct analysis is often difficult or impossible. Charging causes a shift of peak positions, and lateral or depth dependent inhomogenities of the potential cause peak broadening and distortion of spectra. It is therefore important to either find methods for charge compensation, or to determine the magnitude of the surface potential and apply a correction method.

After some basic information on charging of insulators during electron irradiation given in section 7.2.2, a novel method for measuring a positive surface potential of ionic crystals under electron irradiation will be presented in section 7.2.3. In section 7.2.4 and 7.2.5, charging of CaF_2 under a variety of experimental conditions is discussed.

7.2.2 Charging during electron irradiation

The sign of the surface potential of an insulating crystal under electron irradiation depends on the total electron coefficient σ, which is defined as the current of secondary plus backscattered electrons, divided by the current of primary electrons. Depending on the material under investigation and the beam parameters, σ may be larger than 1, which means that a positive surface potential is observed despite of irradiating with negative electrons.

Positive surface charge caused by electron irradiation generally does not exceed a few volts, while negative surface charge can reach values close to the primary beam energy. The magnitude of the total electron (T.E.) coefficient depends on the kinetic energy of the impinging electrons and their angle of incidence. For bulk insulating materials, one observes a low and a high primary energy (called E_{P1} and E_{P2}) were the T.E. coefficient is equal to 1; in the energy range between E_{P1} and E_{P2} it is larger than 1. The surface potential is therefore positive for primary energies between E_{P1} and E_{P2} and negative for other energies. For CaF_2, both values E_{P1} and E_{P2} are not well known. For insulators, the value of E_{P1} generally seems to be of the order of 10 eV, which is about the energy needed to create a valence band hole. As an example, 15 eV were determined for MgO [SSH97]. For electrons of normal incidence, Reimer [Rei93] gives a value of about 2 keV for E_{P2}. In this work, a positive surface potential was observed for electron energies up to 3 keV (limit of the electron source). It was also found

that the effects of beam induced changes of the surface composition have to be taken properly into account.

The magnitude of the surface potential U observed under electron irradiation is determined by the kinetic energy distribution $d\sigma/dE_{SE}$ of the secondary electrons. In a simple model for an ideal insulating material, the primary electron current must be in equilibrium with the backscattered and secondary electron currents after a stationary state is reached. The value assumed by the surface potential U is then given by the condition that the number of electrons with kinetic energies larger than eU equals the number of primary electrons:

$$\int_{eU}^{E_P} \frac{d\,s}{dE_{SE}}\, dE_{SE} = 1 \qquad 7.1$$

The equilibrium condition is illustrated in Fig. 7.1.

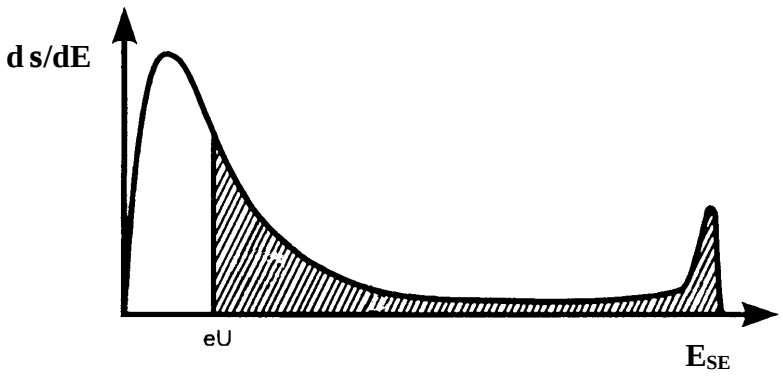

Fig. 7.1 Schematic representation of the total electron kinetic energy distribution $d\sigma/dE_{SE}$, normalized to the primary current [BSR95]. The surface voltage U reaches the equilibrium value when the integral over the shaded area is 1. The integral over the complete distribution curve is the secondary electron coefficient σ for the respective primary electron energy.

If the kinetic energy distribution $d\sigma/dE_{SE}$ of the secondary electron coefficient changes, the sample surface potential will also change in order to maintain the equilibrium condition. During electron irradiation of insulating crystals, changes in the secondary electron coefficient are caused by selective desorption of one ionic species, resulting in a different surface stoichiometry (see below). The equilibrium may also be altered by additional currents to or from the surface, the main contributions in our case are a current through the sample and positive ion desorption. These currents tend to lower the surface potential.

7.2.3 Technique for surface potential determination

In this section, a new method is presented that allows to measure the positive surface potential of an insulating crystal during electron irradiation. A sketch of the experimental setup for surface potential measurement is given in Fig. 7.2.

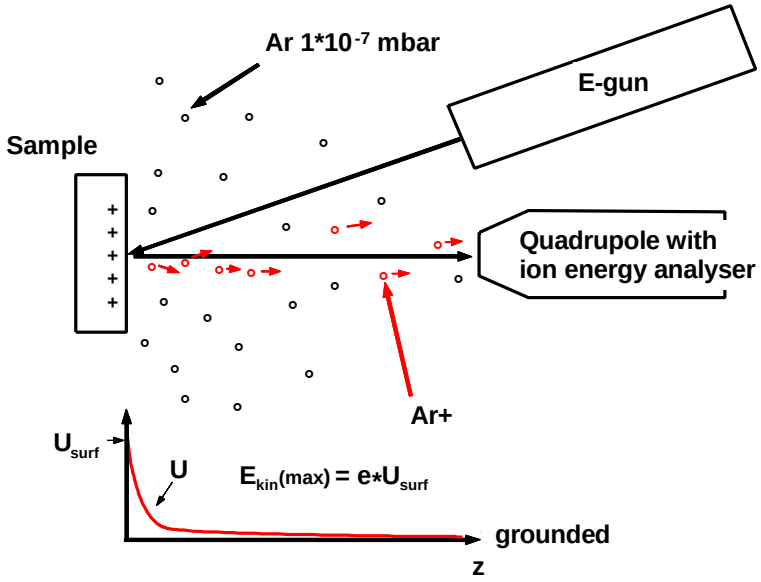

Fig. 7.2. Drawing of the setup used for the determining the surface charge during irradiation. The chamber is filled with Argon at a pressure of $1*10^{-7}$ mbar. Part of the Ar is ionized by primary and secondary electrons. As there is an electric field between the charged sample surface and the grounded quadrupole, the Ar^+ ions gain a certain kinetic energy. Those ions generated directly in front of the charged sample gain the highest possible kinetic energy, $E_{kin}(max) = e*U_{surf}$. Thus, surface charge can be derived from the high energy cutoff edge in the Ar^+ kinetic energy spectra (see Fig 7.3).

In order to determine the surface potential, Argon at a pressure of typically $1*10^{-7}$ mbar is used as charge monitor. Part of the Argon is ionized by primary and secondary electrons in the electric field between the charged sample surface and the grounded quadrupole. Those Argon atoms ionized directly in front of the charged CaF_2 surface are exposed to the highest positive potential and gain the maximum kinetic energy $E_{kin}(max) = e*U_{surf}$. By measuring the kinetic energy spectrum of the Ar^+ ions, the surface potential can be derived from the high energy cutoff edge.

A measurement of the surface potential of a crystal cleaved in UHV that was carried out with this method is shown in Fig. 7.3. The set of data that is presented was recorded under typical irradiation conditions at 1.5 keV primary beam energy and a current density of 12 $\mu A/cm^2$.

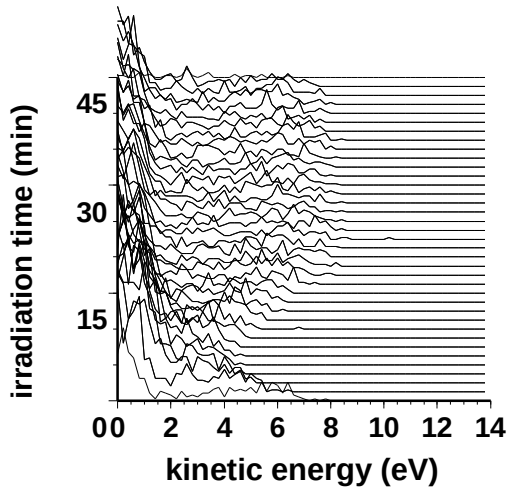

Fig. 7.3 Series of Ar^+ kinetic energy spectra taken during irradiation of a crystal cleaved in UHV. In this three-dimensional representation, the kinetic energy is shown in the x-axis, the y-axis is the irradiation time and the (unlabeled) z-axis shows the ion yield in arbitrary units. This representation is used many times throughout this chapter. The temporal evolution of surface potential can directly be extracted from the high energy cutoff edge according to the formula $E_{kin}(max) = e*U_{surf}$. High maximum kinetic energy means high surface charge. Note that the surface potential is high at the beginning of irradiation, goes through a minimum and increases again. This behavior is found to be typical for UHV cleaved crystals. Primary energy was 1.5 keV at a current density of 12 $\mu A/cm^2$ at RT.

A similar measurement was repeated with a crystal that was cleaved in air. The result is shown in Fig. 7.4.

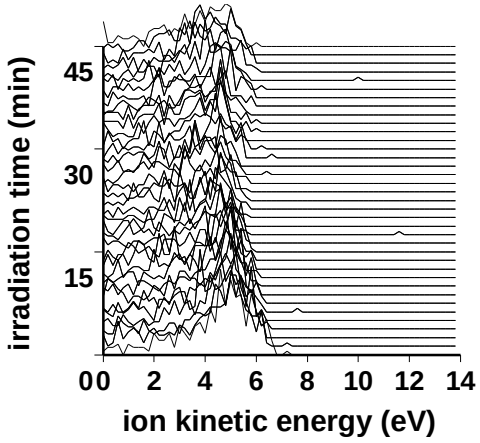

Fig. 7.4 Series of Ar^+ kinetic energy spectra taken during irradiation of a crystal cleaved in air. Primary energy was 1.5 keV at a current density of 18 $\mu A/cm^2$ at RT.

The position of the cutoff edge is obvious from figures 7.3 and 7.4. In order to obtain the temporal evolution of surface potential, this cutoff edge is extracted from the spectra by numerical analysis. The result of this procedure performed for the above two sets of spectra is shown in Fig. 7.5.

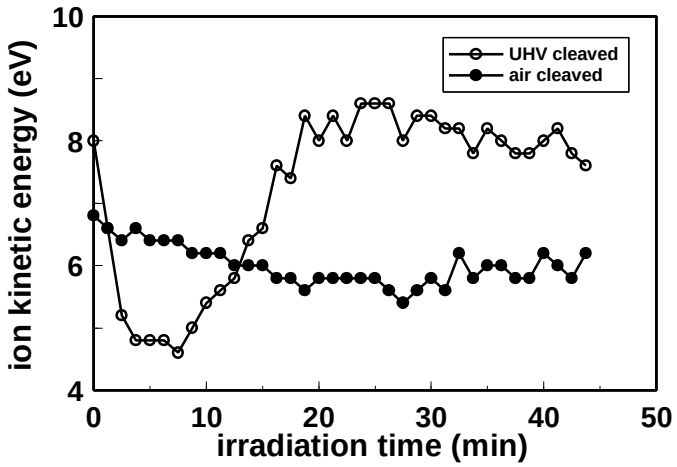

Fig. 7.5 Comparison of the temporal evolution of surface potential of UHV and air cleaved crystals. Irradiation was performed at RT, the primary energy was 1.5 keV. Current density was 12 µA/cm^2 for the UHV cleaved crystal and 18 µA/cm^2 for the air cleaved crystal.

The most interesting observation made here is that the surface potential of crystals cleaved in UHV shows a pronounced minimum about 5 - 15 min after starting irradiation. No such minimum is observed for crystals cleaved in air, instead charging is rather constant in this case. It is shown in the next section that these differences can be understood from the chemical composition of CaF_2 surfaces produced by cleavage in UHV and in air.

7.2.4 The influence of surface stoichiometry on the surface potential

Stoichiometric changes of CaF_2 were induced by electron irradiation, which results in fluorine depletion and metallization of the surface, and by dosage of gases like O_2 and CO_2 during electron irradiation. It is demonstrated that metallization lowers the surface potential, while a high coverage of the surface with nonmetallic species like fluorine or oxygen causes a high surface potential.

In the following two experiments, the influence of the amount of fluorine in the topmost layer on the surface potential is investigated. In the first experiment that was performed at RT, the surface is increasingly metallized during electron irradiation, while the second experiment was

conducted at 670 K, where calcium metal desorbs thermally, thus the surface remains close to a stoichiometric state. As a measure for the coverage of the surface with fluorine, the F^+ ion yield is evaluated, assuming that the ion yield is in first order proportional to the amount of fluorine in the topmost layer. In Fig. 7.6, the surface potential as determined with the Ar^+ method is shown along with an F^+ ion yield curve that was recorded simultaneously.

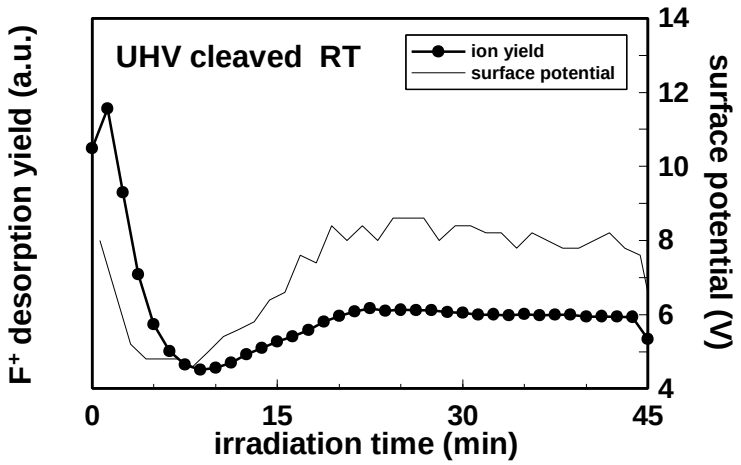

Fig. 7.6 Temporal behavior of F^+ yield and surface potential under irradiation for an UHV cleaved crystal at RT, primary energy was 1.5 keV at a current density 12 µA/cm^2. The surface potential develops parallel to the F^+ ion yield.

Both, surface potential and ion yield reach a minimum after about 8 min of electron irradiation. Fig. 7.7. shows the result of a measurement using the same irradiation parameters, but with the sample at a temperature of 670 K.

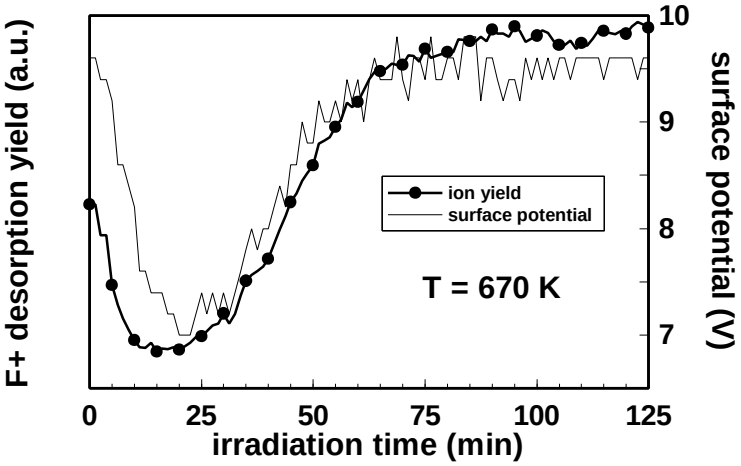

Fig. 7.7 F^+ yield and surface potential under electron irradiation at 670 K. Primary energy was 1.0 keV at a current density of 12 µA/cm^2, the sample was cleaved in UHV.

For both measurements recorded at sample temperatures of 300 and 670 K, surface potential and ion yield exhibit a parallel temporal development. It is concluded that high surface potential and high occupation of the surface with fluorine are correlated for UHV cleaved crystals.

A similar experiment as those shown in Fig. 7.6 and 7.7 was repeated with a crystal that was cleaved in air. The result is shown in Fig. 7.8.

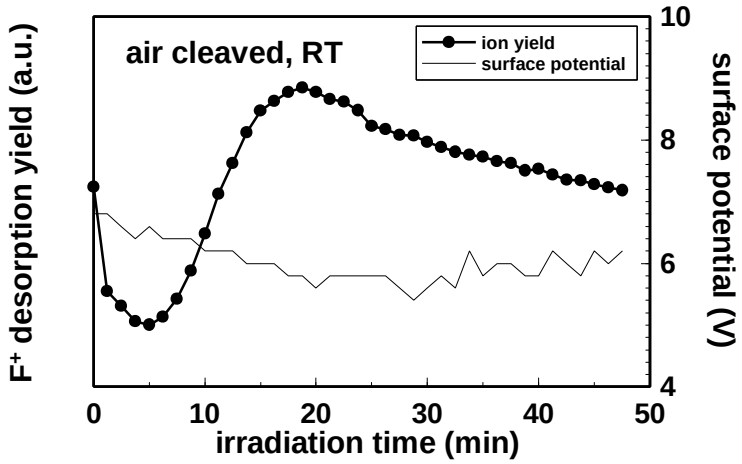

Fig. 7.8 Temporal behavior of F^+ yield and surface charge under irradiation for an air cleaved crystal at RT. Primary energy was 1.5 keV at a current density of 18 $\mu A/cm^2$. The surface potential was constant for the crystal cleaved in air, while the yield showed the same evolution as in the case of the UHV cleaved crystal.

The ion yield shows a similar temporal development for crystals cleaved in air and in UHV, however, the surface potential is does not exhibit a strong variation. The constant surface potential of air cleaved crystals is interpreted as due to contaminants that do not desorb under irradiation. It was shown in Chapter 5 that contamination of air cleaved crystals mainly consists of oxygen from the air. During electron irradiation, nonmetallic CaO forms instead of calcium metal as on UHV cleaved crystals. The influence of adsorbates on the surface potential under electron irradiation can be directly monitored by dosing O_2 or CO_2 to UHV cleaved crystals after about 4-5 min of electron irradiation. Similar effects were observed for both gases. A steplike increase in the surface potential occurred upon dosage.

The magnitude of the step in surface potential for both gases can be derived from Fig. 7.9.

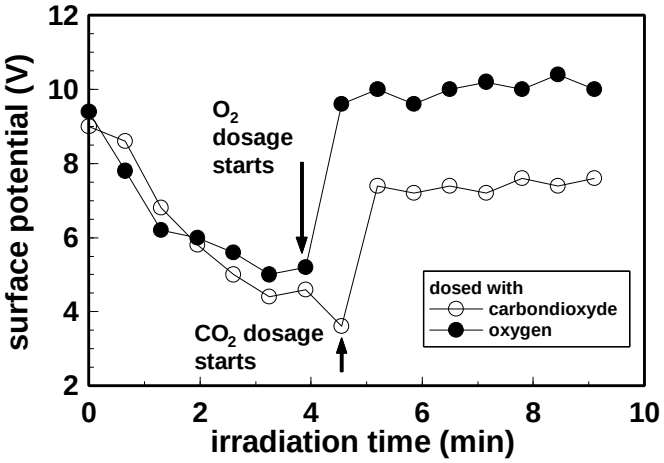

Fig. 7.9 Effects of O_2 and CO_2 dosage on the surface potential. In both cases, gas pressure was $1.5*10^{-7}$ mbar. The potential increases by about 4 V in the case of CO_2 dosage, while after oxygen dosage, a stronger increase of almost 5 V is observed.

It can be seen that oxygen adsorption causes a larger increase in surface potential than does carbondioxyde adsorption. This result confirms again the observation made in measurements conducted with UHV and air cleaved crystals (Figs. 7.3 and 7.4) that the surface potential is sensitive to the chemical composition of the surface. Under continued irradiation, the potential remains constant, even after the oxygen supply was turned off. It is concluded that oxygen does not desorb under electron irradiation.

In conclusion, the experimental results demonstrated that a high degree of coverage of the surface with nonmetallic species like fluorine or oxygen causes a high surface potential. The decrease of the surface potential of crystals cleaved in UHV during the first minutes of irradiation can be understood from fluorine desorption. The increasingly metallized surface has a lower secondary electron coefficient. The subsequent increase of the potential is interpreted as due to diffusion of fluorine from the bulk to the surface.

Some investigations that cover similar subjects can be found in literature and are discussed here, however, due to the lack of work performed on CaF_2, no direct comparison is possible. Irradiation induced changes have been investigated by Golek [Gol94] for KCl and by Hopman et al [HVS97] for rutile (TiO_2). Adsorbate induced changes were treated by Shih and coworkers [SYP97] for diamond surfaces.

The influence of stoichiometric changes on the positive surface potential of KCl under irradiation has been investigated by Golek [Gol94] by recording shifts in Auger electron spectra. The dependence of the surface potential from sample temperature was recorded. Contrary to the results obtained in this thesis, at high temperatures (>600-900 K), a low surface potential of about 2-3 V was found, while in an intermediate region between 400 and 500 K a maximum charging of 6 V was observed. The decrease of the surface potential at high temperature was attributed to thermal desorption of potassium. If this explanation holds, KCl would exhibit just the "inverted" temperature dependent charging behavior of CaF_2.

Hopman and coworkers [HVS97] investigated the temporal variation of the secondary electron coefficient during electron irradiation of rutile (TiO_2). The temporal development of the surface potential was studied in the negative charging region, with the primary energy above the crossover point E_2. The observed beam induced decrease of the SE coefficient was attributed to stimulated oxygen desorption. Similar to this work, depletion of the first layer, and subsequent diffusion of oxygen to the surface were extracted to explain the results. Additionally, an influence of irradiation enhanced conductivity was assumed. However, the processes in the negative charging region are considerably different from those observed for CaF_2 in the positive charging regime.

Adsorbate induced changes of the secondary electron yield have been investigated by Shih et al [SYP97] by comparing clean and hydrogen terminated diamond surfaces. A very high secondary electron yield was found on samples saturated with surface hydrogen.

Summarizing, it is concluded that the questions addressed in this section have also been treated by other groups on different materials, and similar qualitative explanations like desorption of one chemical component of the sample or diffusion, have been evolved. However, the details of the surface potential evolution are considerably different for the various materials and electron primary energies.

7.2.5 Dependence of surface potential on primary energy and beam current

The Ar^+ method was used to obtain the surface potential of UHV and air cleaved crystals under electron irradiation at primary energies ranging from 0.6 to 3 keV. The surface potential was determined from the cutoff edge of the first recorded Ar^+ spectrum taken after starting electron irradiation. The results are displayed in Fig. 7.10.

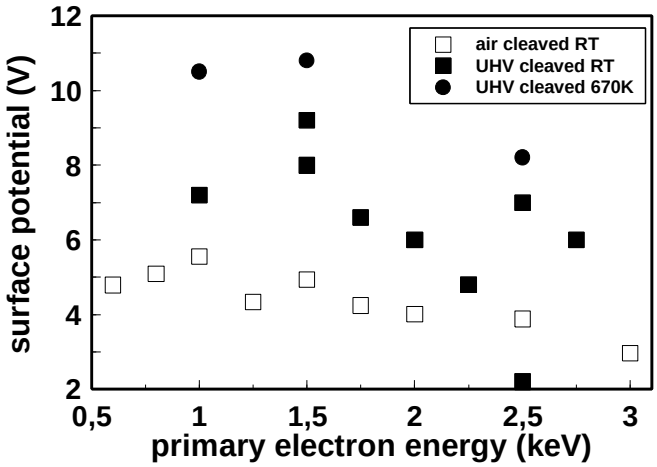

Fig. 7.10 Dependence of the surface potential on the primary electron energy at the beginning of electron irradiation. The maximum of the surface potential occurs around 1 keV primary energy for air cleaved samples and around 1.5 keV for UHV cleaved samples. At elevated sample temperatures, the surface potential was higher. At the maximum available primary energy of 3.0 keV, both surfaces are still positively charged. The dashed line was drawn as a guide to the eye. Current density was 60 µA/cm^2 for the air cleaved samples and 12 µA/cm^2 for the UHV cleaved crystals.

Fig. 7.11 shows the dependence of the surface potential on current density for UHV and air cleaved crystals.

A clear dependence of the surface potential on the primary electron energy (see Fig. 7.10) was found for air cleaved crystals only, while the values obtained from UHV cleaved crystals showed larger scattering but no clear trend. The maximum surface charge was observed at about 1 keV for air cleaved samples and at roughly 1.5 keV for UHV cleaved crystals. At elevated sample temperatures, the surface potential was higher, in accordance with the observations made in Ref. [BSR95].

The general conclusion concerning charging problems that may be drawn from the experiments is that the magnitude of the surface potential is better reproducible for crystals cleaved in air, and charging problems are much less serious in this case. About half of the UHV cleaved crystals did not show the distinct behavior concerning surface potential apparent from Fig. 7.3.

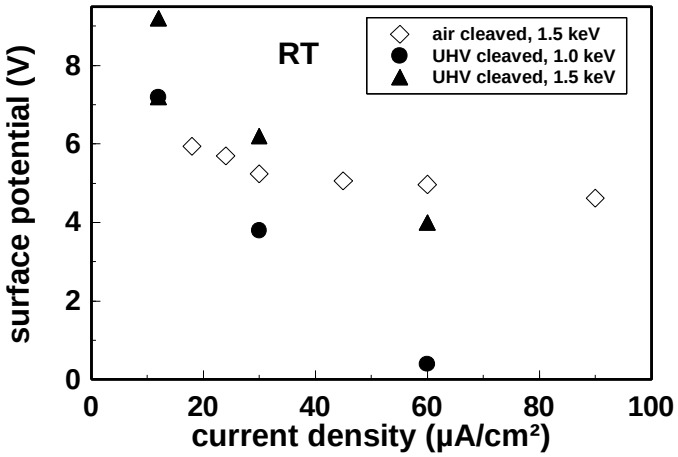

Fig. 7.11 Dependence of the surface potential at the start of electron irradiation on current density for crystals cleaved in UHV and in air. For both surfaces, the potential decreases with increasing current density. Similar to the results shown in Fig. 7.10, UHV cleaved crystals show a much stronger dependence on beam parameters than those cleaved in air. The measurements were performed at RT.

Most deviating results can be summarized in two categories: a) after starting the irradiation, no Ar^+ yield at all is observed, which probably means that the surface potential is negative from the beginning, b) The decrease in surface potential observed during the first minutes of irradiation extents to negative values, thus retracting Ar^+ back to the surface. In both cases, the surface potential did almost never reassume a positive value, and no Ar^+ yield was further observable. The reason for the differences in charging behavior may be unavoidable variations in the cleavage quality, and charge patches originating from cleavage which do not neutralize because of poor crystal-ground contact. The step density differs from cleavage to cleavage, and small splinters of CaF_2 produced during cleavage may stick to the surface with poor electrical contact and influence charging. An influence of the step density on the physical properties of CaF_2 crystals was also found in laser ablation experiments, where it was shown that destruction of the material starts at step edges already at comparatively low laser fluences [Gog97].

7.2.6 Summary and conclusions

A new experimental method was developed allowing the determination of a positive surface potential of insulators under electron irradiation. With the help of this method, it was possible to determine the surface potential of CaF_2 bulk crystals under 0.6 to 3.0 keV electron irradiation. It was demonstrated that the stoichiometry of the sample surface has a strong

influence on the magnitude of the surface potential. Crystals cleaved in air, or UHV cleaved crystals after oxygen dosage exhibit a rather constant surface potential under electron irradiation. UHV cleaved crystals, however, show a strong surface potential variation during the first minutes of irradiation, that is interpreted as an indication for changes of the coverage of the sample surface with fluorine due to desorption and diffusion.

The Ar^+ method should also be applicable to other types of surface analysis of insulators that suffer from positive sample charging, like X-ray photoemission and scanning electron microscopy. As an example, the method may be useful in determining the energy E_2 where the total electron coefficient changes from larger than 1 to smaller that 1 with increasing primary energy, which results in a change from positive to negative surface potential (see chapter 7.2.2). The method most often used in the determination of the crossover point E_2 works as follows [Rei93]: the insulator is covered with a thin gold film except for parallel stripes that are 50 to 200µm wide. Under irradiation in an electron microscope, width and image intensity of the stripes change dramatically when the insulator surface turns negatively. With this method, a crossover energy of about 2 keV was determined for CaF_2 [Rei93]. However, in the present work it was found that the CaF_2 surface is still positively charged when irradiated with electrons of 3.0 keV primary energy (which unfortunately is the upper limit of the electron source). It seems that the sample can be much better characterized when the Ar^+ method is applied because the results reflect the properties of the pure material rather than those of a partially gold covered system.

7.3. Kinetic energy of F^+ ions desorbing from CaF_2

7.3.1 Introduction

Several attempts to measure the kinetic energy distributions of F^+ ions desorbing from CaF_2 during electron irradiation were published in literature. Experiments performed on air cleaved crystals in our group [BSR95], [Rei95] gave high ion kinetic energies of the order of 5 to 10 eV. These results are reflecting mainly the magnitude of positive sample charging under electron irradiation. As the surface potential remained undetermined in these experiments, no information on the intrinsic desorption energies of the ions was obtained. Charging can be reduced by the use of thin epitaxial films evaporated on metallic or semiconducting substrates, and electron stimulated desorption from thin fluoride films was measured by two groups [MSS91], [ZGT94]. However, the results are far from being consistent and it is apparent that the use of thin films does not avoid charging problems in all cases. Hence, the question of intrinsic desorption energies is still open. It will be answered in this chapter.

First, the microscopic mechanism governing electron stimulated desorption from CaF_2 is discussed. In the following section, the Ar^+ method is used to monitor the surface potential during F^+ desorption investigations. By subtracting the portion of the F^+ ion kinetic energy that is caused by surface charge from the total F^+ kinetic energy, the intrinsic ion kinetic energy distribution is obtained. An effect of oxygen dosage during electron irradiation on the intrinsic ion kinetic energy is demonstrated.

7.3.2 Electron stimulated desorption from CaF_2 via the Knotek-Feibelman mechanism

Positive ion emission during ionizing irradiation is observed for a large number of ionic materials. A model for positive ion emission from ionic solids involving inner shell ionization has been developed by Knotek and Feibelman in 1978 [KFe78]. They proposed a process initiated by the excitation of a hole in the highest lying core level of the cation by a primary electron. Since no higher occupied levels exist at the cation, an interatomic Auger decay can take place which reverses the charge state of an anion. The anion is now positively charged and repelled by the Madelung potential (see Fig. 7.12) [KFe79]. Similar Auger decay driven mechanisms were proposed to explain the dissociation of certain molecules by a "Coulomb explosion" [KVV77] and the formation of bulk *F*-centers in alkali halide crystals (the Varley mechanism, [Var54]).

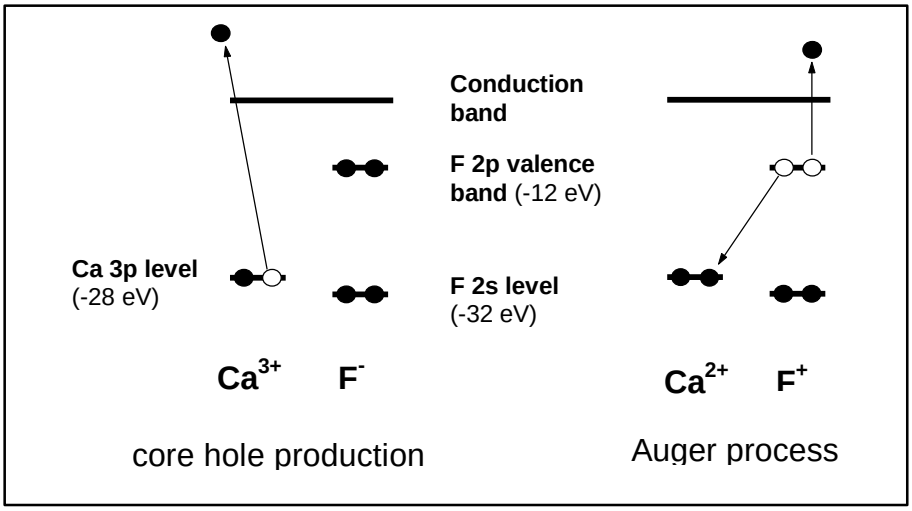

Fig 7.12 Schematic representation of the Knotek-Feibelman process for CaF_2. As a first step, a core hole is produced at the cation 3d level by a primary electron. As there are no higher occupied levels in the calcium ion, an inter atomic Auger decay can take place. One electron from the fluorine valence band fills the calcium core hole. The energy that is gained in this process is used to remove a second electron from the same fluorine. The charge state of fluorine after the process is finished is therefore F^+, and instead of being bound by the Madelung potential, the ion is repelled.

At the first glance, excitation of a F2p core hole should lead to F^+ desorption as well. However, there are two reasons that might prevent F^+ desorption after F2s core excitation. First hand, the lifetime of the two hole state localized at the anion site is a critical factor. Typical times for desorption to occur are about several 100 fs, and it is therefore necessary to have the two holes localized for this time. It was calculated by V. Puchin that this is not possible as long as the F^+ is on the lattice site [Puc98]. The two holes will separate and two V_K-centers are formed. The other and more general reason is a lattice recoil motion that occurs after the charge state of the anion is reversed. This recoil motion has a considerable effect on the desorbing particle kinetic energy. The results of molecular dynamic calculations of the Knotek-Feibelman process suggested [WAv86], [AWa89], [CJe95] that the desorbing particle, instead of being desorbed, may even be recaptured by a rearrangement of the surrounding ions (see Fig. 7.13).

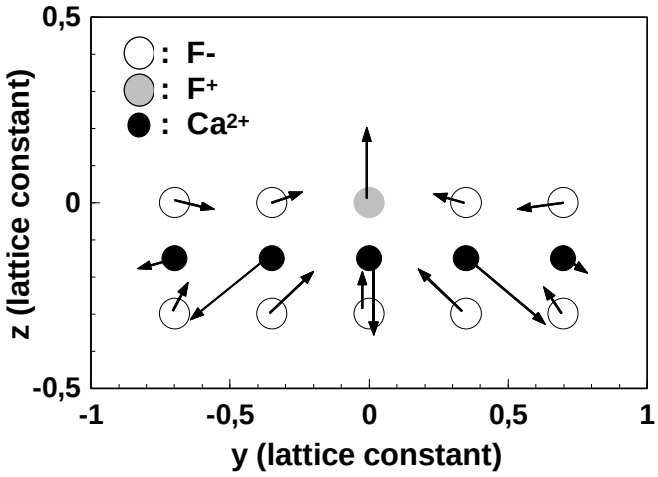

Fig 7.13 Schematic representation of the relaxation movement of ions after charge reversal at a surface fluorine ion according to the calculation of Cieplinski and Jedrzejek [CJe95]. The rearrangement of the neighboring ions may result in an changed potential that becomes attractive for the newly formed F^+, thus preventing desorption.

Walkup and Avouris [AWa89] stated that the Auger desorption mechanism is inoperative for halides with the fluorite structure. Cieplinski and Jedrzejek [CJe95] performed classical trajectories studies and predicted no desorption if the charge state of the anion was reversed while it was still residing on its lattice site. Only after an arbitrary displacement of 0.75 Å towards one of the Ca^{2+} ions, desorption was predicted due to the increased repulsive force. This displacement was intended to simulate an initial movement of the F^- towards the Ca^{3+} during the short time interval between the core hole excitation and the inter atomic Auger process. From this result, it is also clear why desorption of fluorine after F2s core excitation is less probable than after Ca3d core excitation, as the additional electrostatic energy that is gained during the motion of F^- towards Ca^{3+} is not available in this case. Thus, in the light of molecular dynamics investigations, the Knotek-Feibelman process seems to be unlikely to work in CaF_2. If desorption occurs at all, only low ion kinetic energies are predicted.

7.3.3 Charge corrected F^+ kinetic energies

In this section, the intrinsic kinetic energy distribution of the F^+ ions is investigated in detail. To do so, the portion of the ion kinetic energy that is due to surface charge will be subtracted

from the total F^+ kinetic energy using the Ar^+ method to monitor the surface potential during desorption experiments.

During electron stimulated desorption experiments, F^+ and Ar^+ ion spectra were recorded alternatingly, starting with a F^+ spectrum. Recording a single spectrum took about 37 s, after it was completed, an Ar^+ spectrum was taken. The kinetic energy distribution of the F^+ ions is shown in the upper part of Fig 7.14, the corresponding Ar^+ spectra are shown in the lower part.

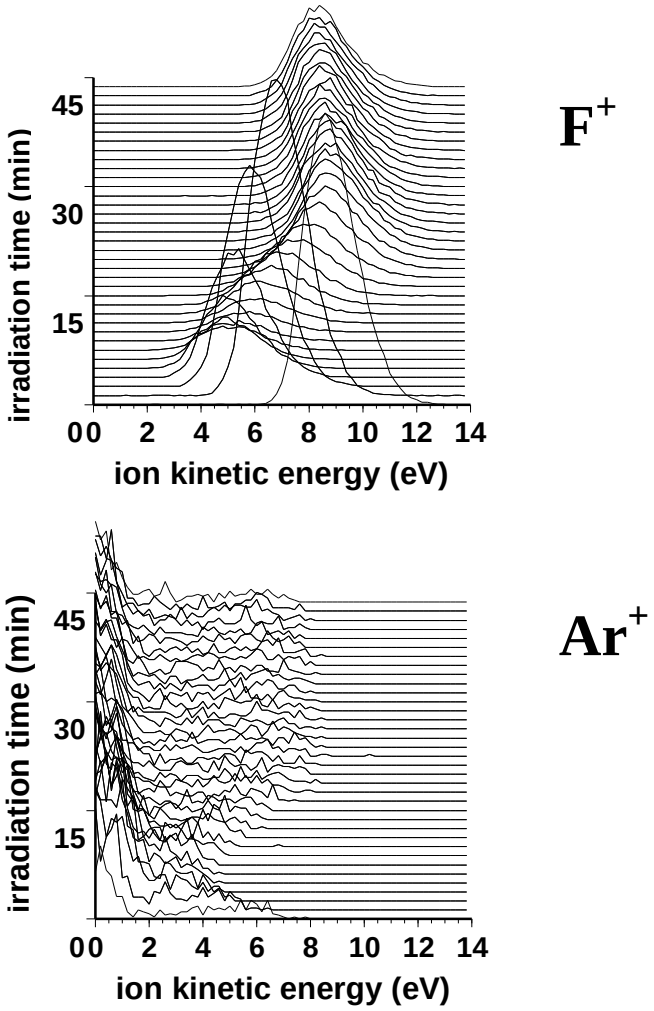

Fig. 7.14 Typical kinetic energy distributions of F^+ and Ar^+ ions taken during electron irradiation. Primary energy was 1.5 keV at a current density of 12 μA/cm^2. The measurement was performed at RT.

From the above two sets of ion kinetic energy distributions, two corresponding F^+ and Ar^+ spectra are shown in Fig. 7.15

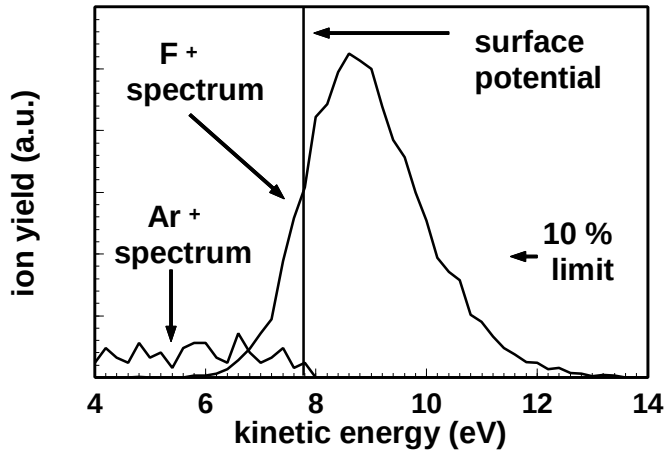

Fig. 7.15 Typical kinetic energy distributions of F^+ and Ar^+ ions taken from the above two sets of measurements. The solid vertical line marks the high energy edge of the Argon spectrum and is a measure for the surface potential of the sample. In this measurement, it is located at 7.8 eV. The peak position of the F^+ kinetic energy distribution is at 8.6 eV. Thus a charge corrected kinetic energy of the F^+ peak of 8.6 - 7.8 = 0.8 eV is obtained. The energy where the F^+ ion yield has decayed to 10 % of the peak is taken as a measure for the width of the distribution. It is indicated by a dashed line. In the figure, it is found at 11.3 eV. Primary energy was 1.5 keV at a current density of 12 $\mu A/cm^2$. The measurement was performed at RT.

The vertical line labeled "surface potential" marks the high energy edge of the Argon spectrum and indicates the highest surface potential present on the sample. Relative to this potential, the peak of the kinetic energy distribution of F^+ ions is found at kinetic energies around 0.8 eV independent from beam current and primary electron energy. The highest ion energies are 4 to 5 eV relative to the surface potential. This is the part of the F^+ kinetic energy that is due to the desorption mechanism. The high energy limit indicated in Fig. 7.15 is used throughout this work as a measure for the width of the distribution. It is defined as the energy where the F^+ yield has decayed to 10 % of the maximum peak yield.

As can be seen in the Fig. 7.15, also F^+ with kinetic energies lower than the Ar^+ threshold is found. There may be two possible explanations for this effect, namely inhomogeneous charging or instrumental broadening. On the first hand, charging may not be uniform within the irradiated spot, but vary laterally to some extent. Since the Argon cutoff edge indicates the highest surface potential present on the sample, low energy F^+ emission from less strongly charged spots would show up with lower kinetic energies. However, from comparison with

desorption measurements performed on thin CaF_2 films evaporated on Si(111), which are believed to exhibit a very uniform charge distribution, it is concluded that the surface potential of bulk crystals under electron irradiation is quite homogeneous (see Fig. 7.16).

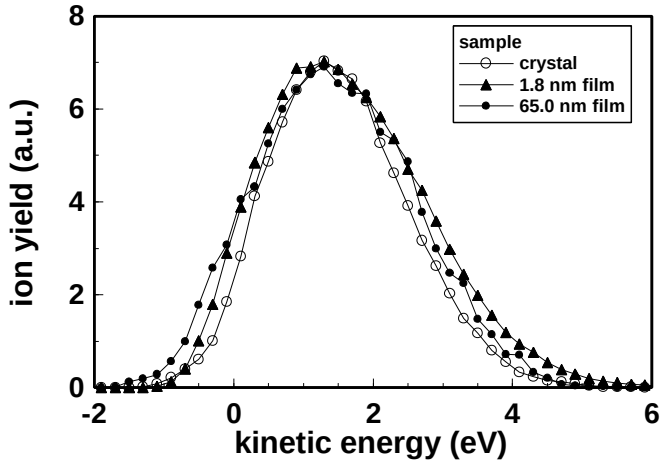

Fig. 7.16 Kinetic energy spectra of F^+ taken from an UHV cleaved crystal and two thin epitaxial CaF_2 films evaporated on Si(111). Spectra from crystals are not broadened compared to those obtained from thin films. It is concluded that surface charge on crystals under electron irradiation is homogeneous. The measurements were performed at RT, primary energy was 1.5 keV at a current density of 12 $\mu A/cm^2$. Spectra were normalized in height and shifted to the same energy.

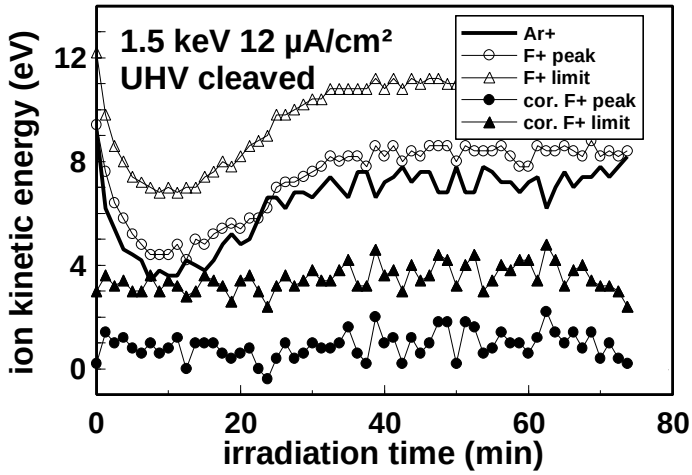

Fig. 7.17 UHV cleaved crystal: charge corrected kinetic energies of the F^+ peak and high energy limit (defined as the energy were the ion yield is 10% of the peak maximum) during prolonged electron irradiation (1.5 keV, 12 $\mu A/cm^2$ at RT). The development of the surface potential is characterized by the minimum at about 10 min after starting the irradiation. The corrected F^+ kinetic energies are not affected by the variations in surface potential.

It is concluded that broadening due to the energy resolution of about 1 eV of the energy analyzer of the mass filter accounts for the effect, as it tends to overestimate the maximum Ar^+ energy and to underestimate the minimum F^+ energy. With the help of the method developed above, the kinetic energy distribution of F^+ was investigated under various experimental conditions. From the F^+ spectra, the position of the maximum was taken and, as an estimate for the highest ion kinetic energies, a high energy limit defined as the energy where the yield amounts to 10% of the peak value. The F^+ kinetic energies corrected for surface charge where then obtained by subtracting the portion of the kinetic energy due to surface charge from the total F^+ kinetic energies as shown in Fig. 7.12.

It was already pointed out in section 7.2 that the surface potential of the UHV cleaved sample shows strong variations during the first minutes of electron irradiation. As can be seen in Fig. 7.17, the corrected kinetic energy of F^+ is not influenced by this effect, it remains constant during the whole time of the experiment (even up to 150 min, corresponding to a total electron dose of 0.1 C/cm^2).

F^+ ions desorbing from crystals that were cleaved in air roughly have the same energy than those desorbing from UHV cleaved crystals (see Fig 7.18). The ion kinetic energy also remains constant during the whole time of the experiment. A transient behavior of the surface potential

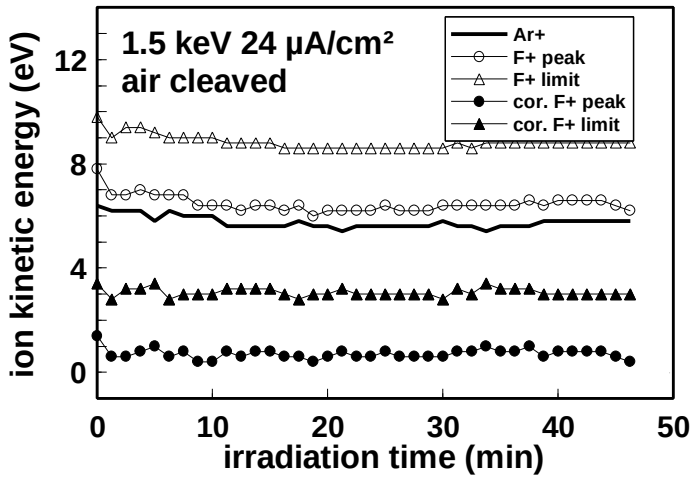

Fig. 7.18 Air cleaved crystal: charge corrected kinetic energies of the F^+ peak and high energy limit during prolonged electron irradiation. These curves reflect the typical behavior of desorbing particle energies from air cleaved crystals. Note that the surface potential is almost constant, in contrast to the much more dynamic development found for UHV cleaved crystals. (1.5 keV, 24 µA/cm^2 at RT).

is observed for UHV cleaved crystals only, but not for those cleaved in air. However, from a comparison of the Figs 7.17 and 7.18, it can be concluded that these differences do not influence the charge corrected ion energies. For the purpose of this chapter, the development of the surface potential with irradiation time is therefore ignored.

The surprising observation made here is that the intrinsic ion kinetic energies are neither influenced by the increasing metallization accumulated during electron irradiation nor by impurities present on air cleaved crystals.

An explanation for the lack of stoichiometric effects in both cases may be obtained from scanning force microscopy (SFM) pictures. On air cleaved surfaces, a large number of small clusters are present that are not found on UHV cleaved surfaces [Ben97]. The impurities caused by cleavage in air form aggregates on the surface, with possibly clean areas between the aggregates. Similar, on the images from electron irradiated surfaces, calcium metal was found to form colloids with apparently uncovered areas between them [RWB96], [BRM97]. The observation that the ion kinetic energies are unaffected by impurities and metallization could be explained by assuming F^+ desorption from the undamaged patches. During prolonged irradiation, the surface colloids grow and cover the fluoride patches, which decreases the desorption yield. However, since no information on the chemical composition of the surface can be given with SFM, it is not clear whether the flat areas between metal or impurity clusters

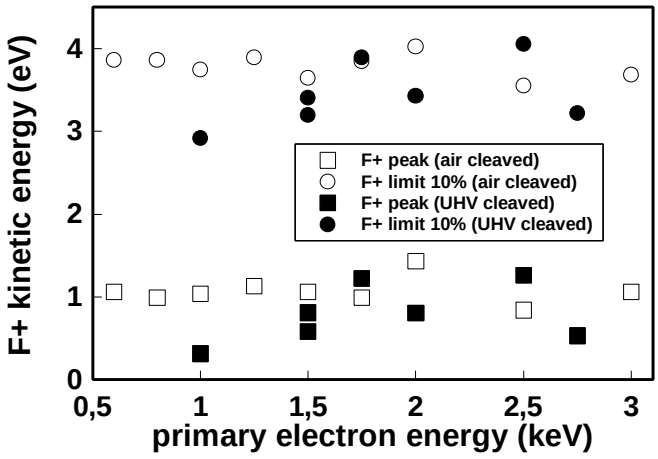

Fig. 7.19 Charge corrected kinetic energies of F^+ ions desorbing from air and UHV cleaved surfaces. The ion kinetic energies are neither influenced by primary electron energy, nor by the differences in surface stoichiometry that subsist between air and UHV cleaved crystals. All experiments have been performed at RT. Current density was 60 µA/cm^2 for the air cleaved crystals and 12 µA/cm^2 for the UHV cleaved crystals.

are really undamaged CaF_2 or not. The interpretation given here is therefore speculative. The corrected kinetic energy (averaged over the first 50 min of irradiation) of the F^+ ions does not depend on the primary electron energy (Fig. 7.19).

The average of the peak energy is 0.9 ± 0.3 eV for the UHV cleaved crystals and 1.1 ± 0.2 eV for the air cleaved crystals. Within the error bars, the kinetic energies of F^+ ions desorbing from air and UHV cleaved CaF_2 surfaces is the same.

The corrected ion kinetic energies determined in this investigation can be compared with experimental results published in literature. The mixed material $Ca_{0.6}Sr_{0.4}F_2$ on Si (111) was investigated by Zanetti et al [ZGT94]. Their F^+ kinetic energy distribution has its maximum at 1 eV, the highest energies extend up to 5 eV. The ion kinetic energy distribution is similar to the one found in the present work in both absolute kinetic energy and width of the distribution. However, the material investigated by Zanetti et al was different from pure CaF_2.

The F^+ kinetic energies measured by Miura and coworkers [MSS91] are higher, their peak is at about 4 eV, a result that is probably caused by charging of their "thick" film.

Compared to findings of theoretical work, the ion kinetic energies observed in this investigation are rather high. The reason for the failure of the theoretical prediction may be inappropriate choice of the starting conditions of the calculation. While the Knotek-Feibelman process starts with the excitation of the Ca3d core hole, the calculation starts with charge reversal from F^- to F^+ on the lattice site. In particular, the movement of the F^- ion towards Ca^{3+} after Ca3d core hole excitation is not taken properly into account. This effect would increase the kinetic energy of the desorbing particle [JCe95].

Additionally, the differences between experimental and theoretical results could be caused by excitonic effects that have so far not been considered in the calculations. An enhancement of the F^+ yield was observed by Eberhardt et al [ECG92] after photoexcitation of the F1s core exciton. It was speculatively argued in this publication that the excitonic electron takes part in the desorption process as a spectator electron, thus changing the magnitude of the recoil motion in a way that the ion is able to escape. However, the exact nature of the process is still unclear.

7.3.4 Influence of surface stoichiometry on desorption energies

As an important result of this work, it was found that gases that were dosed to UHV cleaved crystals during electron irradiation have indeed an important impact on the desorbing ions kinetic energy. In these experiments, O_2 and CO_2 were dosed after about 5 min of electron irradiation. At this time, about 50 % of the surface fluorine ions have desorbed (compare section 7.5). In Fig. 7.20, the result for a UHV cleaved crystal dosed with oxygen is shown.

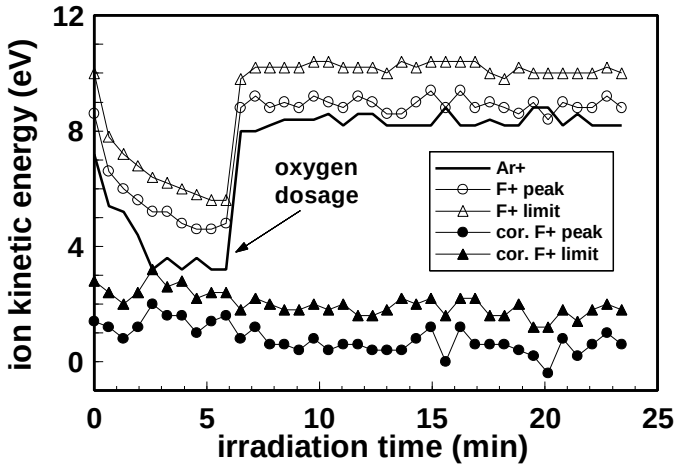

Fig. 7.20 Charge corrected kinetic energies after dosage of oxygen during electron irradiation (1.5 keV, 12 µA/cm^2 at RT). Oxygen dosage at a pressure of 1.5*10^{-7} mbar was started after 6 min of irradiation time and was finished at 13 min. The development of the surface potential is characterized by a steplike increase upon oxygen dosage. The average of the corrected F^+ peak energies before oxygen dosage is 1.4 ± 0.4 eV, while after dosage, an average of 0.6 ± 0.4 eV was determined. The upper limit was 2.6 ± 0.4 eV before and 1.8 ± 0.3 eV after dosage.

It can be seen in the figure that the charge corrected energies do change upon dosage. The average of the charge corrected kinetic energy before dosage is 1.4 ± 0.4 eV, after oxygen dosage, the kinetic energy dropped to an average of 0.6 ± 0.4 eV. Generally, the average ion kinetic energy values were found to decrease by 0.8 to 0.9 eV upon dosage, irrespectible whether the dosed gas was O_2 or CO_2.

The decrease of the ion kinetic energy after oxygen dosage is interpreted as caused by the altered lattice recoil motion. The replacement of the vacancies or surface *F*-centers by oxygen or CO_2 alters the local environment of the remaining surface fluorine ions. The adsorbed particles also take part in the recoil motion that occurs after charge reversal of a neighboring

fluorine from F^- to F^+. However, as mass and charge state of the adsorbate are different from fluorine, the portion of the kinetic energy dissipated in the changed environment is different. This explains the difference in the desorbing ions kinetic energy after dosage.

7.3.5 Summary

In the electrons stimulated desorption experiments presented in this chapter, surface potential and F^+ kinetic energy were measured simultaneously. The intrinsic kinetic energy of F^+ ions desorbing from CaF_2 via the Knotek-Feibelman process was obtained by a procedure correcting for the energy contribution due to the surface potential. For UHV cleaved crystals, the peak of the charge corrected kinetic energy distribution was at 0.9 ± 0.3 eV.

In experiments with controlled stoichiometric changes, gases were dosed on the partially fluorine depleted surface. An influence of the chemical composition of the surface on the ion kinetic energies was found. As an explanation, it was assumed that the energy dissipated in the recoil motion is different when adsorbates are present on the surface, thus a change in the desorbing particle kinetic energy occurs.

7.4. Field driven diffusion

7.4.1 Introduction

An interesting observation made in the investigation of F^+ desorption yield is the occurrence of not only an exponential decay at the beginning of the experiment, but also of a second, delayed peak. This second peak is interpreted as an effect caused by field driven diffusion of fluorine from the bulk to the surface where desorption occurs.

Similar diffusion phenomena during electron irradiation of CaF_2 were investigated by Reichling [Rei95]. In this work, the production of Ca metal, that was monitored by measuring the reflectivity, was found to have the maximum directly after starting irradiation. In contrast to this observation, the F^+ yield attained a maximum only after a certain delay. The delay was interpreted as the time necessary for fluorine to diffuse from the depth of maximum defect creation to the surface where desorption takes place. Diffusion of ions in the irradiation induced field inside the sample was investigated by Ibara et al [ICT95], [ICR96]. In the first study, sodium ion diffusion in glass was found to be strongly influenced by the beam induced field. The second study investigated field driven diffusion in polyvinyl chloride and CaF_2. However, these experiments were performed on gold covered samples in the electron microscope, with much higher beam energies than those used in this work. Field driven diffusion in calciumfluoride under similar experimental conditions as used in this work was considered by R. Bennewitz [Ben97] to explain electron stimulated desorption and gas bubble formation in CaF_2. It was pointed out that defects of opposite sign are separated in the field, which prevents recombination and thus enhances stable point defect production.

In the present work, the ion yield from crystals with a strong internal field and thin films with a small internal field is compared. Field driven diffusion is closer investigated for air cleaved crystals, since in this case the surface potential is rather constant and the situation therefore less complicated than for crystals cleaved in UHV.

7.4.2 Electron irradiation induced field inside the crystal

So far, in this work only the surface potential was considered. For the discussion of charged defect diffusion, also the irradiation induced field inside the crystal has to be taken into account. The representation given here follows mainly the discussion given by Cazaux [Caz86]. The typical field inside the crystal resulting from electron irradiation in the primary energy range where the total electron coefficient is larger than one is shown in Fig. 7.21. A double charge layer builds up in the crystal. Positive surface charge extends to a depth that is assumed to be roughly 3-4 nm, while the deeper region up to the penetration depth of the primary electrons is negatively charged. Note that this charge distribution implies two inversion points P_1 and P_2 where the corresponding electric field E changes sign. Charged defects experience a force in the field in a direction determined by the sign of their charge and their position relative to the inversion points.

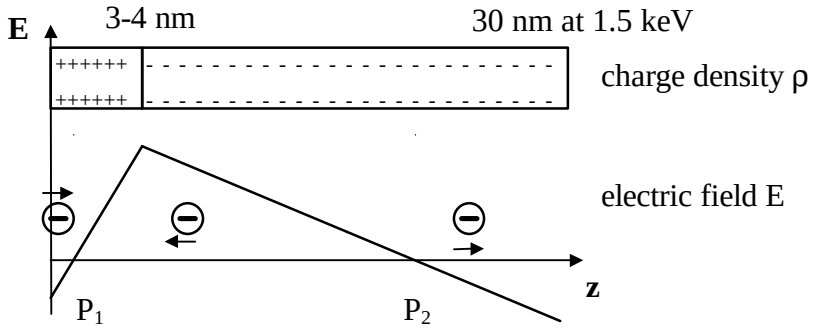

Fig 7.21 Electric field inside the crystal under electron irradiation [Cas86]. In the upper part of the figure, the charge density during irradiation is shown schematically. In the lower half, the resulting electric field is depicted. At the inversion points P_1 and P_2 the field direction changes. Diffusion directions for negatively charged defects (for example I-centers) are shown. Note that for the transport to the surface, negatively charged particles have to overcome a small barrier near the surface (left hand side from P_1).

In the electric field shown in Fig. 7.21, positively charged defects like vacancies are driven into the region close to the inversion point P_2, while negatively charged defects like I-centers are depleted in this region and driven towards the inversion point P_1, or deeper into the bulk of the crystal. The observation of structures interpreted as fluorine gas bubbles made in [JCh83] and [Ben97] was explained by I-center diffusion into the bulk where F_2 gas is formed. It is important to note that I-centers that are created in the region between the two inversion points and that are driven towards P_1 by the field have to overcome a potential barrier (left hand side from P_1) to arrive at the surface.

7.4.3 Temporal evolution of ion yield of crystals and thin films

The influence of the electrical field on F^+ ion yield is evident by comparing an ion yield curve measured from a UHV cleaved crystal, where a strong surface potential was observed, with an ion yield curve obtained from a thin epitaxial CaF_2 film where charging is very small (Fig. 7.22).

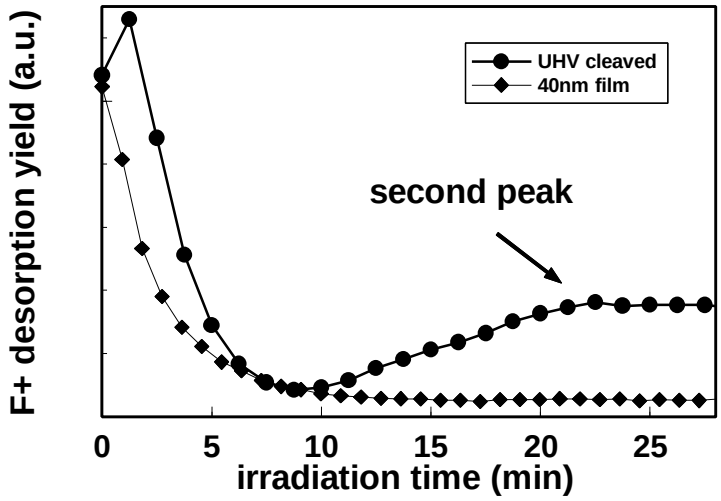

Fig. 7.22 Temporal development of F^+ yield for an UHV cleaved crystal and a 40 nm epitaxial CaF_2 film. The F^+ yield from the UHV cleaved crystal increases again after going through a minimum at about 9 min irradiation time. The ion yield from the thin film exhibits an exponential decay within the time interval shown in the figure. The measurement was performed at RT, primary energy was 1.5 keV at a current density 12 $\mu A/cm^2$.

The observed development of the F^+ yield is taken to reflect depletion or enrichment of the surface layer with fluorine. The decrease in ion yield observed for both samples during the first minutes of irradiation is straightforward to understand from a depletion of the surface layer. After about 15 to 20 min, the ion yield measured from thin films reaches a constant level that is attributed to concentration gradient driven diffusion of fluorine from the bulk to the surface. The increase in ion yield after about 10 min of irradiation time that is observed for UHV cleaved crystals (labeled "second peak" in Fig. 7.22), but not for thin films, is attributed to field driven I-center diffusion from the bulk to the surface. Reaching the surface, the I-centers occupy regular lattice sites, thus replacing desorbed fluorine. This substitution mechanism explains the temporal development of the ion yield.

Two series of measurements were performed on air cleaved crystals, in order to investigate the influence of primary energy and current density on diffusion of fluorine to the surface. In the next figure, it can be seen that the second peak arrives later for increased primary electron energy (Fig. 7.23).

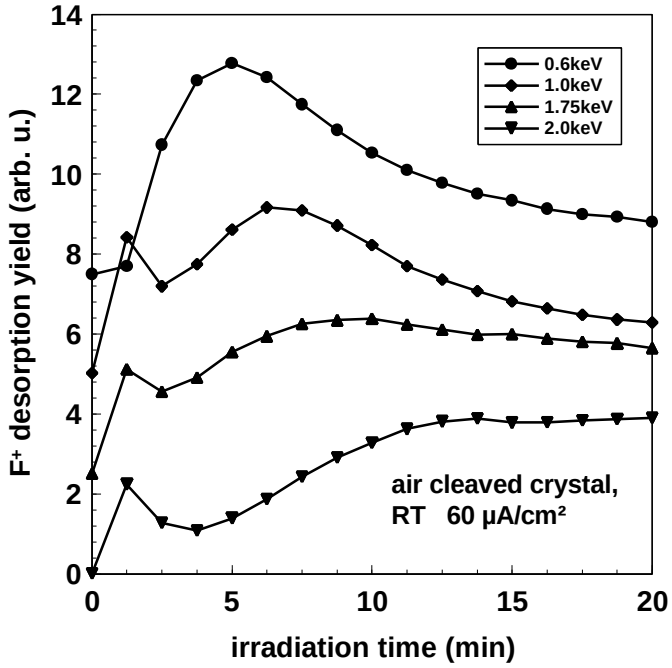

Fig. 7.23 Primary energy dependence of the desorption yield from air cleaved crystals under irradiation at 60 µA/cm^2 current density at RT. With increasing primary energy, the second peak arrives later, and the first peak becomes broader and decreases in yield. These observations reflect the greater penetration depth of the primary electrons and the reduced energy deposition in the upper layers for higher electron energies (compare Fig 2.13). Between successive curves, an offset of 2.5 arb. u. was added.

Increasing the primary energy results in a smaller and slower decaying first peak, and the second peak arrives later. This dependence from primary electron energy can be qualitatively understood from the energy deposition curves shown in Fig. 2.13. The energy deposition near the surface is smaller for high primary energies, and the maximum of energy deposition dE/dx is found in greater depth. The arrival time of the second maximum in ion yield is interpreted as the time I-centers formed in the depth of maximum energy deposition need to diffuse to the surface. To check this interpretation, the arrival time of the second maximum in ion yield as a function of the primary electron energy is given in Fig. 7.24, along with a calculated curve from [BSR95], indicating the depth of the maximum in the energy deposition curve dE/dz for the respective primary electron energy (compare Fig. 2.13.).

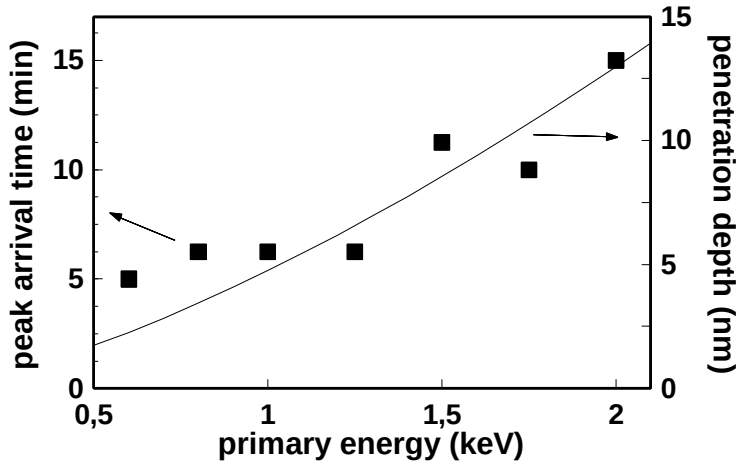

Fig. 7.24 Primary energy dependence of the arrival time of the second maximum in F^+ yield. At higher primary energy, the second peak arrives later. The solid curve gives the depths of the maximum in energy deposition according to the penetration depths calculation of [BSR95]. Air cleaved crystal, 60 $\mu A/cm^2$ current density at RT.

From a comparison of both curves, it is concluded that the arrival time of the second maximum can indeed be understood as the time fluorine needs to desorb from the depths of maximum defect creation to the surface. These interpretation is similar to the one developed by

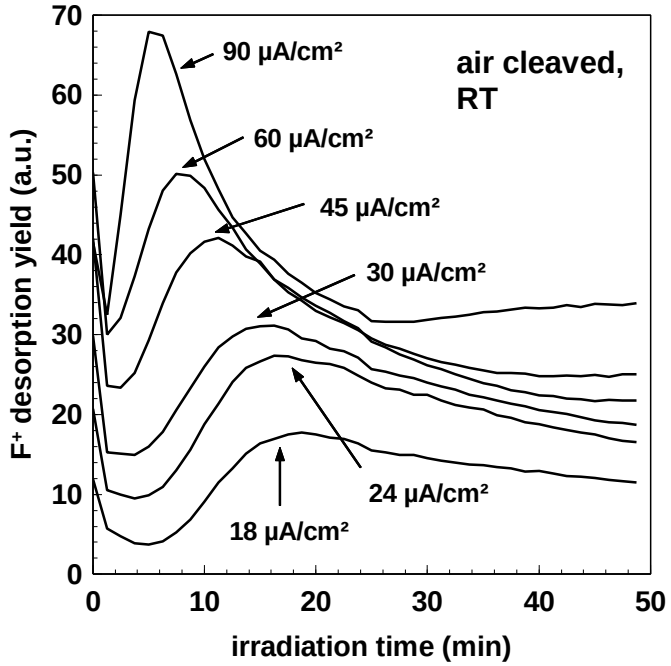

Fig. 7.25 Current density dependence of the desorption yield from air cleaved crystals under irradiation with electrons of 1.5 keV primary energy at RT. With increasing current density, the second peak arrives earlier. The surface potential corresponding to these measurements is shown in Fig. 7.10. An offset of 4 a.u. between successive curves was added for better discernibility.

Bennewitz et al [BSR98] in their investigation of bulk and surface processes in electron irradiated CaF_2. Furthermore, a strong influence of the primary current density on the arrival time of the second ion yield maximum was observed. The corresponding series of measurements is shown in Fig. 7.25.

With increasing current density, not only the F^+ yield increases, but the second peak arrives earlier. Interpreting this observation in terms of the field driven diffusion model, one is lead to assume a stronger internal field for increased current density. The magnitude of the surface potential, however, is only a slowly varying function of current density (compare Fig. 7.11). Thus, the relationship between surface potential and internal field is not simply linear when increasing the current density. Since so far only a rough qualitative understanding of the electric field inside the crystal is available, no interpretation for the observed current density dependence can be given.

The results concerning surface potential and stoichiometry presented in chapter 7.2 and the observation made in this chapter can be interpreted within a joint picture. For the discussion give here, it is assumed that at fixed current density, a high surface potential corresponds to a high internal field.

The results of chapter 7.2 and 7.4 may be summarized as follows: A high amount of fluorine on the surface causes a high surface potential, which under the assumption made here corresponds to a high internal field. A high internal field enhances fluorine transport to the surface. As a consequence of the efficient transport, the amount of fluorine on the surface remains high. It is thus proposed that a high surface potential stabilizes itself via field driven diffusion. In a similar way, if for some reasons the surface potential became negative, this state also stabilizes as in this case I-centers are repelled by the field and fluorine transport to the surface is prevented. This interpretation accounts for the observation that the surface potential of UHV cleaved crystals after several minutes of electron irradiation either increased again (Fig. 7.5 to 7.7) or decreased to negative values (compare section 7.2.5.).

7.4.4 Summary

In the present work, evidence for the influence of the electric field on desorption yield is obtained by comparing the results from bulk crystals and charge free thin films. The dependence of field driven diffusion on primary electron energy was discussed qualitatively. It was proposed that a high surface potential stabilizes by enhanced field driven diffusion.

7.5. Desorption from epitaxial CaF_2 films

7.5.1 Desorption from thin epitaxial CaF_2 films

The intention behind the investigation of thin epitaxial CaF_2 films evaporated on Si (111) was to observe a gradual transition from the charge free state expected for very thin films to the complex charging behavior of UHV cleaved crystals for films thicker than the penetration depth of the primary electrons. However, it turned out that a completely different behavior is observed.

No dependence of the ion kinetic energy on film thickness in the investigated range from 3 to 65 nm was observed. It is concluded that even 65 nm thick CaF_2 films do not charge under 1.5 keV electron irradiation.

The temporal evolution of the ion yield under electron irradiation was different from those observed for bulk crystals. As an example of F^+ desorption from films, Figs. 7.26 and 7.27 show ion kinetic energy distribution curves measured from a 40 nm thick CaF_2 film evaporated on Si (111).

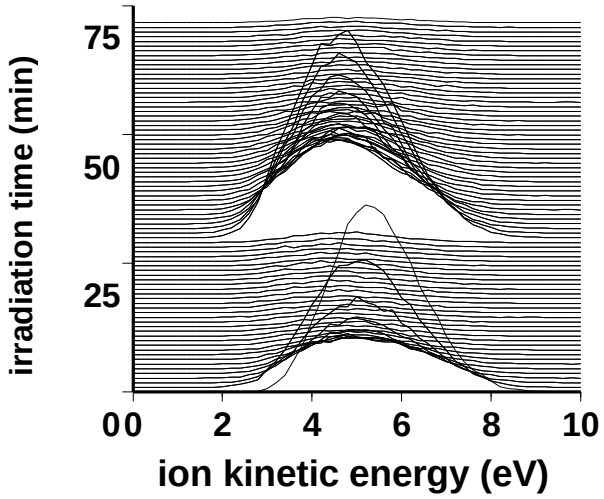

Fig. 7.26 F^+ kinetic energy distribution curves from a 40 nm CaF_2 film evaporated on Si(111). In contrast to the smooth second peak observed for crystals, a steplike increase in desorption yield is found to be typical for thin films. Current density was 12 $\mu A/cm^2$, primary electron energy was 1.5 keV, the experiment was performed at T=370 K.

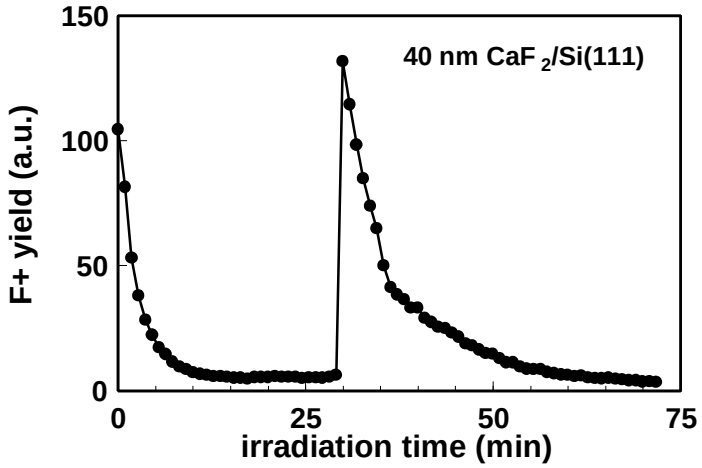

Fig. 7.27 Desorption yield from a 40 nm film CaF_2 evaporated on Si (111). Current density was 12 μA/cm^2, primary electron energy was 1.5 keV, the experiment was performed at T=370 K.

The sudden increase in desorption yield was observed for film thicknesses ranging from 3 to 65 nm. In different experimental runs, the arrival time of the feature ranged from 15 to 30 min. It did not depend on film thickness. The steep increase is assumed to be caused by spontaneous contraction of a metallic surface layer. After a sufficient amount of fluorine has desorbed from the surface layers, an increasingly metallike film of several layer thickness forms. This film becomes unstable and contracts to form colloids, since colloid formation is

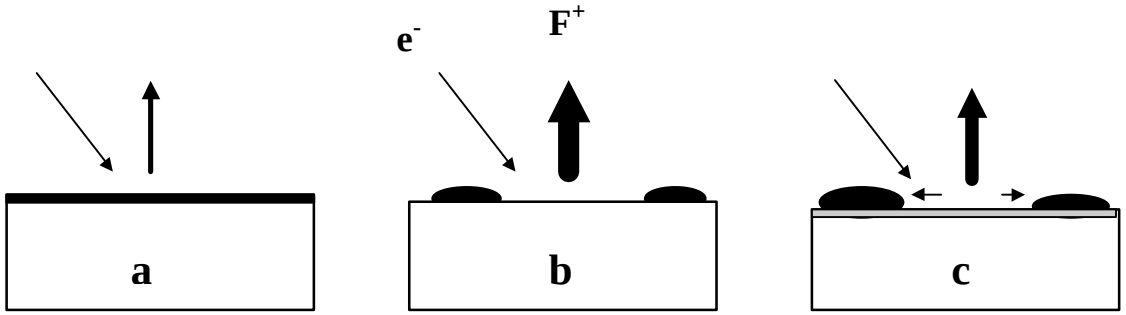

Fig. 7.28 Schematic drawing of the surface metallization of a thin CaF_2 film under electron beam exposure. After several minutes of irradiation, most fluorine in the near surface region has desorbed and a metallic Ca film has formed on the surface (a). Due to the high surface energy of Ca, this film becomes unstable and contracts into colloids. Fluorine rich material is exposed to the incident electrons and a sudden increase in F^+ yield is observed (b). During continuing irradiation, the colloids grow by collecting *F*-centers and Ca atoms that diffuse on the surface (c). This prevents the formation of the metallic layer for a second time.

energetically favored as the surface energy of Ca metal (about 1 J/cm^2 [Ben97]) is higher than for CaF_2 (0.46 J/cm^2 [Tas80]). The colloids cover a much smaller area than the metal film, so fresh material is exposed to the beam, resulting in a steplike increase in F^+ desorption yield. Metal and *F*-centers produced in the uncovered area during subsequent irradiation can diffuse into the colloids (Ostwald ripening). This prevents the repetition of the steplike increase, as no further closed Ca-film builds up again. This model is schematically summarized in Fig. 7.28.

The exponential decay of the yield that is observed during the first minutes of electron irradiation can be used to calculate the cross section σ_{ESD} for the desorption process. It is assumed that the observed ion yield is proportional to the coverage Θ of the surface. For thin films, the exponential decay is not disturbed by a contribution from field driven diffusion as was observed for crystals. The time dependent surface coverage can therefore be expressed by the following exponential law:

$$\Theta = \Theta_0 \exp -(\frac{s_{ESD} * j * t}{e}) \quad 7.2$$

From the gradient of the graphs in Fig. 7.29, the cross sections for three film thicknesses are calculated. For the 1.8 nm thick film, the highest cross section of $2*10^{-16}$ cm^2 has been determined, for the 12 nm film the cross section was $1.0*10^{-16}$ cm^2 and for 65 nm $2.25*10^{-17}$ cm^2. The increase of the cross section with decreasing film thickness is likely due to primary and secondary electrons that are backscattered or reflected at the CaF_2/Si interface.

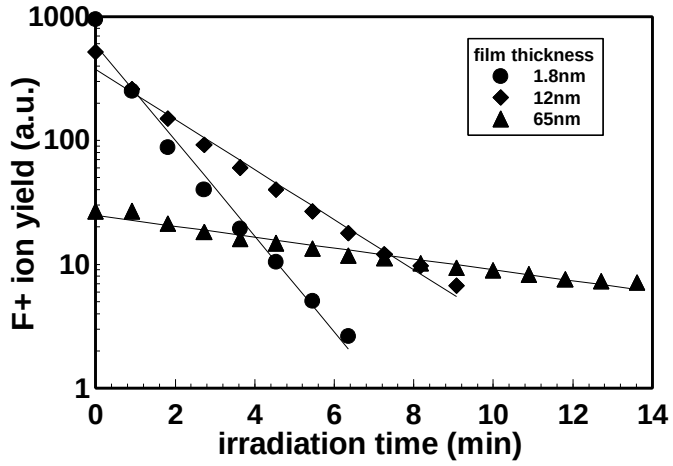

Fig. 7.29 Exponential decay in F^+ yield during the first minutes of irradiation. Solid lines represent fits to the data. The calculated cross sections for F^+ desorption are: 1.8 nm film: $2*10^{-16}$ cm^2, 12 nm film: $1.0*10^{-16}$ cm^2, and 65 nm film: $2.25*10^{-17}$ cm^2.

A value for the cross section for fluorine desorption under electron irradiation has been obtained by Strecker et al [SMG81]. For their 2.5 keV electrons, they estimated an effective cross section for fluorine desorption of about $7.5*10^{-19}$ cm^2. The value was determined from the variation of the fluorine Auger signal strengths with irradiation time. From the cross section, a critical dose of 0.21 C/cm^2 was calculated assuming a 10 % detectable change in the fluorine concentration within the probed volume. According to more recent investigations, this value is much to high, which in turn means the cross section determined by Strecker et al is too low. Saiki et al [SSA87] observed surface damage under 150 eV electron irradiation at only 10 $\mu C/cm^2$. From their data, a cross section of $1\text{-}1.5*10^{-15}$ cm^2 for 150 eV electrons can be estimated.

In Fig. 7.30, the ion kinetic energy distribution from a 24 nm thick film is shown at three irradiation times. A gradual increase in energy is observed.

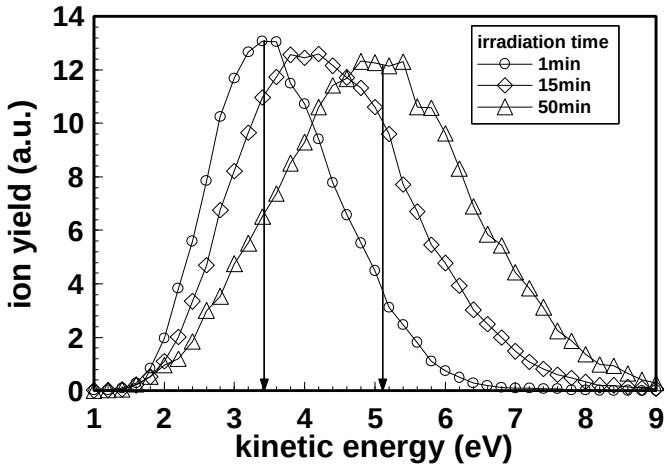

Fig. 7.30 Kinetic energy distributions of F^+ ions desorbing from a 24 nm thick CaF_2 film. While in literature thin films are usually assumed to be charge free, it can be seen that the kinetic energy of the desorbing ions does change with irradiation time. In the present experiment, a shift by about 1.7 eV was observed during 50 min of electron irradiation. This effect is attributed to a decrease in the work function that is caused by calcium metal accumulation during irradiation. Spectra were normalized to the same height. The spectrum at 15 min was the first after the steplike increase. Primary energy was 1.5 keV at a current density of 12 $\mu A/cm^2$. The experiment was performed at a temperature of 400 K.

The effect that causes a change in ion kinetic energies is different from those observed for bulk crystals, where the secondary electron coefficient was the quantity that determined the surface potential. In thin films, the secondary electron coefficient does not influence surface charge,

since the film is in electrical contact with the substrate. The observed increase in ion kinetic energy with irradiation time is attributed to accumulation of defects and Ca metal on the surface of the film. A calcium film on the surface of CaF_2 will result in a more positive contact potential and thus higher ion kinetic energies [DMK97]. As a conclusion, the position of the ion kinetic energy distributions measured from thin CaF_2 films have to be interpreted with care, as irradiation induced work function changes affect the result. This effect is often overlooked in literature [MSS91], [ZGT94].

7.5.2 Summary

In F^+ desorption investigations performed on thin films, a steplike increase in ion yield was observed after about 15-30 min of irradiation time. This sudden increase was attributed to spontaneous contraction of a metallic calcium film at the surface which exposes undamaged material to the beam.

The cross section for electron stimulated fluorine desorption was found to decrease with increasing film thickness. For thin films, electrons backscattered at the CaF_2-Si interface were assumed to contribute to the desorption yield. For a 65 nm epitaxial film evaporated on Si(111), a desorption cross section of $2.25*10^{-17}$ cm^2 for excitation with 1.5 keV electrons was determined.

With increasing surface metallization, a shift of the ion kinetic energy distribution to higher kinetic energy was observed. It was concluded that work function changes caused by metallization affect ion energies measured from thin CaF_2 films. Kinetic energy distributions measured from thin films can therefore not be regarded simply as obtained under charge free conditions, as was done in literature [MSS91].